Magnesium Technology 2012
Edited by: Suveen N. Mathaudhu, Wim H. Sillekens, Neale R. Neelameggham, and Norbert Hort
TMS (The Minerals, Metals & Materials Society), 2012

Hot Formability Curves for Four AZ31B Magnesium Alloy Sheets Obtained by the Pneumatic Stretching Test

Fadi Abu-Farha[1], Ravi Verma[2], Louis G. Hector, Jr.[2]
[1]Department of Automotive Engineering, Clemson University; 4 Research Drive; Greenville, SC 29607, USA
[2]GM R&D, General Motors; 30500 Mound Road; Warren, MI 48090, USA

Keywords: Formability, Composite FLDs, Mg AZ31B, Pneumatic Stretching Test, Orientation Effects

Abstract

The formability of four Mg AZ31B sheets produced by either direct chill or twin roll continuous casting, and having different initial grain sizes, was investigated at 400 °C and $5x10^{-3}$ s^{-1} using the pneumatic stretching test. Blanks were pneumatically bulged through four elliptical die inserts, with aspect ratios ranging between 1.0 and 0.4, producing ellipsoidal domes with different biaxial strain combinations. Testing was carried out in two ways: with the major strains being aligned either along or across the rolling direction of the material. Strain combinations were measured in the deformed specimens, and the forming limit curves were constructed for each of the four sheets in two orientations. The results show great impact of sheet orientation on material formability limits. Additionally, the results reveal significant differences between the four sheets; those differences were correlated back to disparities in grain structure and material inhomogeneities.

Introduction

Increasing demand for more fuel efficient vehicles is driving mass reduction in new vehicle designs. This is not surprising since an excess of 50% of total fuel consumption is found to be mass dependent; a fact that is stimulating interest in lightweight alloys. The low density of magnesium alloys, in particular, makes them ~35% lighter than aluminum alloys and ~78% lighter than steels. In spite of the significant weight-savings promised by magnesium alloys, their use in automotive components is predominantly found in die castings. Poor formability of wrought magnesium alloys, hampered in part by limited room temperature ductility owing to strong crystallographic texture and the large anisotropy between basal and prismatic slip, has precluded broader use of these materials. Basal slip and twinning of the HCP crystal structure of magnesium are the only active deformation mechanisms at room temperature [1]; thus, elevated temperature forming processes are needed to activate the five independent slip systems required by the von-Mises criterion. In addition, other diffusion-assisted mechanisms, such as grain boundary sliding and dislocation climb, may become relevant at elevated temperatures [2]. The most common wrought magnesium sheet alloy is the AZ31B, the elevated temperature forming of which has been directed towards vehicle closure panels [3]. A considerable increase in the ductility of this alloy occurs above 200-225 °C [4-6]; therefore, practical use of the alloy is generally realized through either warm stamping (~200-300 °C) [7] or hot pneumatic forming (~300-450 °C) [3].

Critical to any sheet metal forming operation are forming limit curves (FLCs); empirical relationships between major and minor biaxial strains that describe the limits of sheet formability [8-9]. Accurate FLCs are essential for finite element (FE) simulations of sheet forming, since they establish the boundaries between successful forming and failure. Mechanical stretching tests, according to the Marciniak [10] and Nakazima [11] methods are the most common procedures for measuring sheet formability limits, and they are standardized in ASTM E2218 [8] and ISO 12004 [12]. While these formability tests have been extensively applied in the literature, several issues affect their applicability and accuracy. Frictional effects are difficult to eliminate, even under well-lubricated conditions. The Marciniak test, in particular, is designed to have minimal frictional effects through the use of a carrier blank that isolates the deforming specimen from the punch; yet several examples can be found in the literature where material failure takes place away from the center of the deformed specimen [13]. On the other hand, available equipment for mechanical stretching tests is generally limited to ~300-350 °C [13-15]; this precludes their use in studying the hot formability of lightweight Al and Mg alloys. Moreover, these sheet alloys are often formed pneumatically at high temperatures (400-550 °C) via superplastic forming (SPF) or its lower temperature variant quick plastic forming (QPF); therefore, mechanical stretching tests do not resemble the actual loading conditions the material undergoes during pneumatic forming operations. Finally, it is important to construct the FLCs at near-constant strain rates, since high strain rate sensitivity is expected at warm and high temperatures; the latter is not easy to achieve in mechanical stretching tests since they are mainly carried out at constant punch speeds.

The "pneumatic stretching test" resolves most of the issues encountered in mechanical stretching tests, although with some limitation on the extent to which major/minor strain space can be readily sampled. It is based on the free bulging of sheet specimens through a series of elliptical die inserts, thus producing material deformation at different biaxial strain ratios. The latter can be evaluated by circle grid analysis (CGA) or digital image correlation (DIC) to construct the material's FLCs. The test can be conducted at near-constant strain rates, at very high temperatures, and without the significant frictional effects associated with mechanical stretching tests. In previous efforts, the test was validated by investigating the formability of the AA5083 at selected hot forming conditions [16]. The test was also used to construct the first set of "composite FLDs" which show the effects of sheet orientation on material formability limits for both AA5083 and Mg AZ31B sheets [17]. In this study, the pneumatic stretching test is employed in a detailed investigation on the hot formability (at 400 °C and 5×10^{-3} s^{-1}) of four Mg AZ31B sheets. The sheets, some of which have been the subject of earlier studies [18-19], have the same composition; however, they were produced through either twin roll continuous (TRC) casting or direct chill (DC) casting and underwent distinct processing routes, resulting in differences in their nominal grain sizes. A composite FLD was generated for each of the four sheets; disparities in their formability limits were related to differences in their initial microstructures and material inhomogeneities.

Experiments

Materials and Specimen Preparation

The four Mg AZ31B sheet materials, which we arbitrarily label as (A, M, N and O), have similar compositions, as detailed in Table I. They were received in the O-temper condition, with a nominal thickness of ~1mm. Sheet (M) was produced by DC casting, while the other three sheets were produced by TRC casting. Standard microstructural examination was performed on specimens taken from each sheet; the resulting optical micrographs are shown in Figure 1. Analysis of the latter revealed that sheets (A, N and O) (all of which were produced by TRC casting) have similar average grain size (d_{avg} = ~5 μm). Sheet (M), on the other hand, was found to have an average grain size of ~10 μm; nearly twice as large as that of the other three sheets.

Table I. Composition, manufacturing process and average initial grain size of the four Mg AZ31B sheets investigated in this study.

Sheet	Composition (%)				Process (Casting)	d_{avg} (μm)
	Al	Zn	Mn	Mg		
A	2.8	0.81	0.30	Balance	TRC	5.3
M	2.6	0.71	0.32	Balance	DC	10.0
N	3.0	0.74	0.35	Balance	TRC	4.9
O	3.0	0.74	0.32	Balance	TRC	4.8

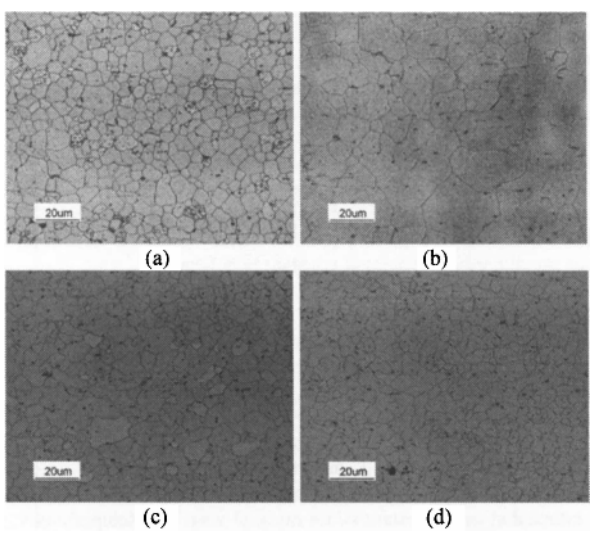

Figure 1. Optical micrographs of the four Mg AZ31B sheets investigated in this study: (a) A (b) M (c) N (d) O.

In preparation for testing, the sheets were first cut into ~100mmx100mm (4"x4") square blanks using a hydraulic shear. Each blank was lightly polished using 400 grit sanding paper, maintaining polishing consistency with the rolling direction of the sheet. Lectroetch LNC-3 solution was then used to electrochemically etch a 2.54mm (0.1") circular grid pattern on the surface of each blank. Particular attention was given to aligning the grid with the sheet's rolling direction; this is crucial for correlating the major and minor strains in the deformed specimen with the longitudinal and transverse directions of the sheet. This is also important for accurately establishing the relationship between a specific sheet orientation and the obtained FLCs, as will be detailed in later sections.

Testing Setup

The core of the setup is the forming die assembly, which is detailed in Figure 2. A die body provides the base on which one of multiple die inserts can rest. A blank is secured between the die insert and the die cover, and a 15-25 kN clamping force seals the chamber on top of the blank in preparation for testing (bulging). Four elliptical die inserts were used in this work to generate different biaxial strain ratios in the deformed specimens. The inserts share the same major axis of 63.5mm (2.5"); the minor axis varies progressively to produce four die aspect ratios (k=1.0, 0.8, 0.6 and 0.4). All inserts were prepared with a die entry radius of 4.76mm (0.1875"), in order to facilitate sheet deformation and minimize the possibility of premature failure along the die insert's perimeter. The forming die assembly is secured to a universal load frame, and enclosed within a custom-built heating chamber (furnace) capable of achieving temperatures in excess of 700 °C. Further details about the pneumatic stretching test setup can be found in earlier publications [16-17]

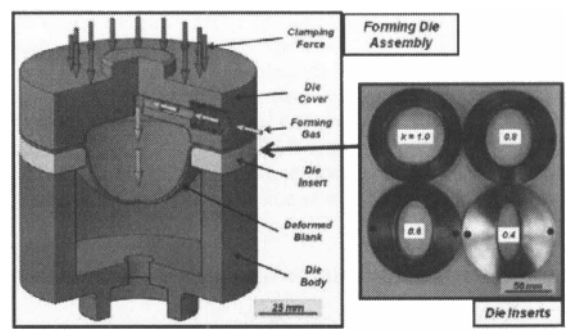

Figure 2. Pneumatic stretching test setup.

Material Deformation Rate

Control of sheet deformation rate to near-constant levels is essential in this test, and it is accomplished by varying the pressure of the forming gas accordingly. The latter is typically achieved through finite element simulations; yet due to the simplicity of the die inserts, an analytical approach was followed here. The closed-form solution for free bulging into elliptical die inserts, derived by Banabic et al. 2001 [20], describes the necessary gas pressure-time (P-t) profiles as follows:

$$P(t) = \frac{2s_0\bar{\sigma}}{b_0 a_0}\frac{\left(1+\alpha k^2\right)}{\rho} e^{\frac{-3\dot{\bar{\varepsilon}}t}{2\rho}}\left(e^{\frac{2-\alpha}{2\rho}\dot{\bar{\varepsilon}}t}-1\right) \quad (1)$$

$$k=\frac{b_0}{a_0},\ \alpha=\frac{1}{2}\left(1+e^{1-\frac{1}{k}}\right),\ \rho=\sqrt{1-\alpha+\alpha^2} \quad (2)$$

where P is the forming pressure, t is the forming time, $\bar{\sigma}$ is the effective stress, $\dot{\bar{\varepsilon}}$ is the effective strain rate, s_0 is the initial sheet thickness, a_0 and b_0 are the major and minor half axes of the elliptical die insert, respectively. Using the above equations, the P-t profiles required for forming the four Mg AZ31B sheets, at a selected temperature of 400 °C and effective strain rate of $5x10^{-3}$ s^{-1}, were obtained. The required flow stresses were obtained using the Sellars-Tegart hyperbolic sine equation [21]. Details on the fit to the hyperbolic sine equation for various Mg AZ31B sheets covered in this study can be found in Dryer et al. 2009 [18].

Testing Procedure

The entire forming die assembly is first heated to 400 °C and allowed to equilibrate for a minimum of 60 minutes. A blank is then inserted, and 5 minutes are allowed to guarantee thermal equilibrium. Towards the end of the heating period, the forming die assembly is closed, and the clamping force is applied in preparation for testing. A test is then begun by the introduction of the forming gas (Argon in this case) following the P-t profile for the selected material and the corresponding die insert. A test is ultimately terminated when sheet rupture is detected; the latter is sensed by a sudden drop in the applied pressure. The deformed blank is then retrieved and another testing cycle is started over. At least two tests were performed for each material/die insert to assure repeatability of the results.

Finally, to investigate the effects of sheet orientation on material formability limits, forming experiments were carried out in two orientations: (1) In the first, sheet specimens were positioned in the forming die assembly such that the rolling direction was aligned with the minor axis of the elliptical die insert (which is the direction of major strains); domes formed under this condition and the corresponding results are denoted by "0° orientation". (2) In the second, sheet specimens were positioned such that the rolling direction was transverse to the minor axis of the elliptical die insert; domes formed under this condition and the corresponding results are denoted by "90° orientation".

Results and Discussion

After pneumatic testing and deforming the sheet specimens into ellipsoidal domes, circle grid analysis (CGA) was performed on each dome to measure the planar strains associated with the deformed grid elements (deformed circles). The collected strain data points were distinguished by deformation zone (safe, marginal and failure); this is important for delineating the material FLCs, and was accomplished by following the ASTM E2218 guidelines [9]. The concept of a "composite FLD" was recently introduced as a comprehensive tool (formability map) for quantifying orientation effects on the formability limits of the material [17]. The latter is constructed here for sheet (A) in Figure 3. Note that (for each of the two orientations) the lower "green" curve was drawn such that most of the safe data points fall below it; similarly, the upper "red" curve was drawn such that most of the failure data points lie above it.. This plot clearly shows that the material exhibits greater formability limits in the 0° orientation over those in the 90° orientation. Although the curves meet in the balanced biaxial region, this composite FLD indicates that ~20% increase in the major strains can be achieved in the 0° over the 90° orientation, as the strain state moves toward the plane-strain condition. Should this composite FLD be plotted in terms of the engineering strains, a difference of more than 30% between both orientations is observed.

Similar detailed analysis was carried out on the remaining three AZ31B sheets, and the results are summarized in Figure 4. While the general trends noted for sheet (A) were similarly observed in the other sheets, disparities were found to exist among the four sheets. Close examination of Figure 4a (0° orientation) and Figure 4b (90° orientation) shows that sheet (A) exhibits the highest formability limits of all four magnesium alloy sheets in both orientations. Sheets (M) and (O) follow with nearly equal formability limits, although sheet (O) exhibits higher limits in the 90° orientation. Finally, sheet (N) is found to exhibit the lowest formability limits of all four sheets, regardless of the biaxial strain ratio and/or sheet orientation.

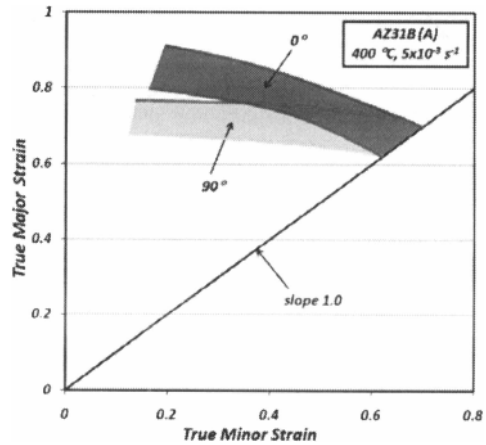

Figure 3. A "Composite FLD" for the Mg AZ31B sheet (A) showing its FLCs in both the 0° and 90° orientations.

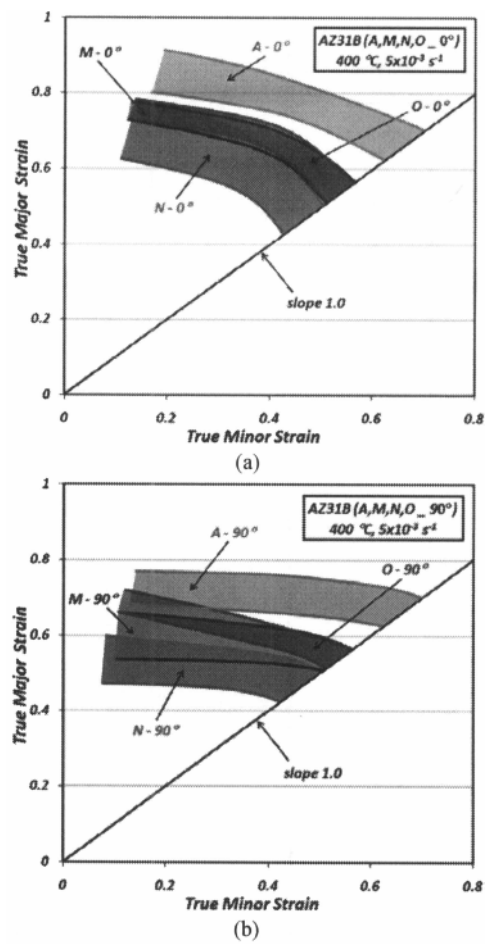

Figure 4. A direct comparison between the FLCs of the four Mg AZ31B sheets in the (a) 0° orientation (b) 90° orientation.

An example of a quantitative comparison between the formability limits of the four Mg AZ31B sheets is provided in Table II, for the balanced biaxial strain region (along the line with slope = 1.0). The major limiting strain (ε_{major}) is extracted for each sheet by considering the average of the safe and failure FLCs (median of each zone in the figure). The effective limiting strain ($\varepsilon_{effective}$) is equal to twice the value of the major limiting strain (ε_{major}), based on von-Mises. The extracted results indicate that sheets (M) and (O) exhibit ~15% higher formability over sheet (N), while sheet (A) exhibits ~40% higher formability over sheet (N). Similar comparisons can be performed at other biaxial strain ratios.

Table II. Comparison between the limiting strains for the four Mg AZ31B sheets at k = 1.0 (according to the FLCs in Figure 4).

Sheet	ε_{major}	$\varepsilon_{effective}$	% change in $\varepsilon_{effective}$ with respect to sheet (N)
A	0.66	1.32	40.4%
O	0.54	1.08	14.9%
M	0.54	1.08	14.9%
N	0.47	0.94	----

The impact of sheet orientation on material formability limits can be also observed through examination of the maximum dome height prior to failure; the latter is plotted in Figure 5 below.

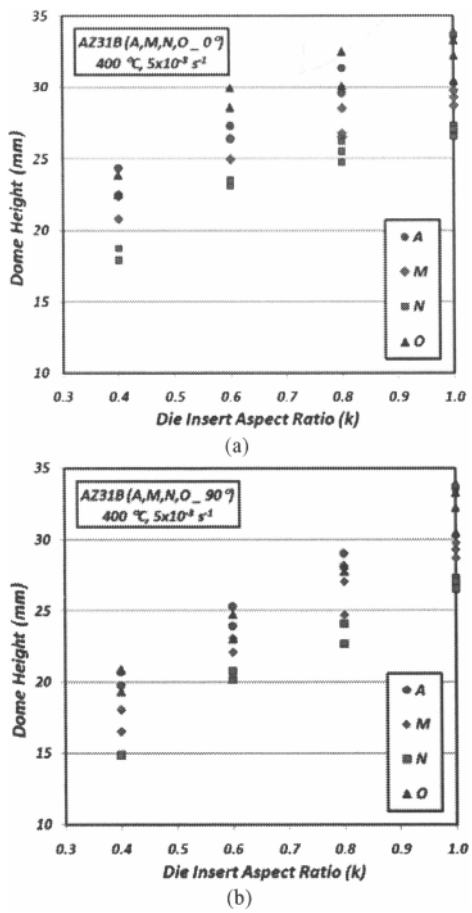

Figure 5. A direct comparison between the four Mg AZ31B sheets in terms of the maximum dome height: (a) 0° (b) 90° orientation.

The trend observed here is found to be consistent with the formability limit results in Figure 4, except in the case of sheet (O). Note that sheet (O) achieves greater dome height values than those achieved by sheet (M). In fact, the dome heights achieved with sheet (O) exceed those recorded for sheet (A) in the 0° orientation (Figure 5a). Since sheet (A) clearly achieves higher limiting strains than sheet (O) (according to Figure 4), the higher dome heights observed with sheet (O) must be the results of more uniform deformation (thickness distribution) in the latter compared to the former. To verify this hypothesis, equivalent domes formed from each of the two sheets at k = 1.0 were considered. Images that show cross-sectional profiles in Figure 6 indicate that the dome formed out of sheet (O) is closer to a semi-circular contour than the dome formed out of sheet (A). Moreover, by taking thickness measurements across each of the two domes, the profile corresponding to sheet (O) was found to exhibit more uniformity (i.e. less thinning) relative to that of sheet (A), as demonstrated by the lower part of the figure.

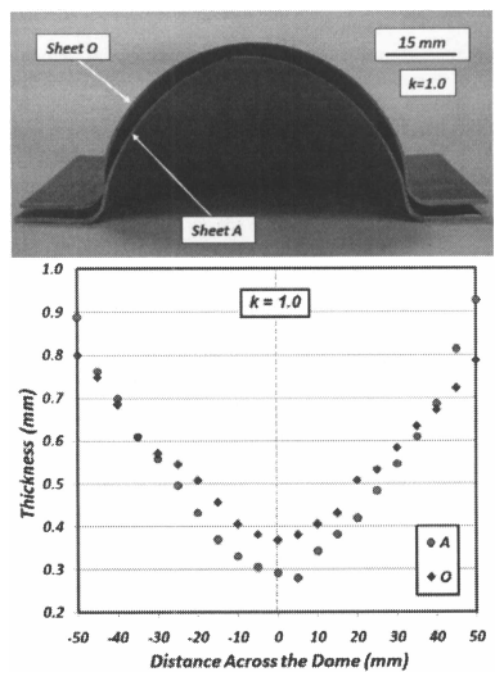

Figure 6. Section views of two domes formed at k = 1.0 from sheets (A) and (O), and the corresponding thickness distributions.

In summary, the results presented so far suggest that sheet (A) is the most formable of the four Mg AZ31 sheets, while sheet (O) exhibits more uniform deformation. Since the chemical composition and initial grain structure of these two materials are similar, the discrepancy in their behaviors can be attributed to the differences in sheet rolling practices of the different suppliers. The formability of sheet (M), which is the only material prepared by DC casting, falls behind that of sheets (A) and (O); this is expected, given its generally larger initial grain size (see Figure 1 and Table I). As for sheet (N), having a fine-grained structure (which was shown to be similar to those of sheets (A) and (O)) does not justify its significantly-lower formability limits, especially in comparison with sheet (M), which has a larger initial grain size. Consequently, further examination was carried out to explain this discrepancy.

Qualitative examination of domes formed from the four Mg AZ31B sheets showed that sheet (N) exhibits remarkably less uniform deformation, accompanied by significant surface damage that's evident over a large portion of the formed dome. An example illustrating the observations in regard to sheet (N) is given in Figure 7, which shows a dome formed at k = 0.8 in the 90° orientation. Note the excessive surface damage and fracture over multiple locations across the surface of the dome. Clearly, rupture does not occur near the dome pole as expected from the pneumatic stretching test. It is speculated that this could be a result of internal material defects that promote premature sheet rupture. A common defect that can lead to premature sheet failure under elevated temperature forming conditions, such as the ones employed in this study, is the clustering of second phase particles [22-23]. A TRC cast sheet with its limited rolling reduction is more prone to this kind of defect than a DC cast sheet. The multiple failure locations seen in the domes formed with sheet N is suggestive of this kind of defect.

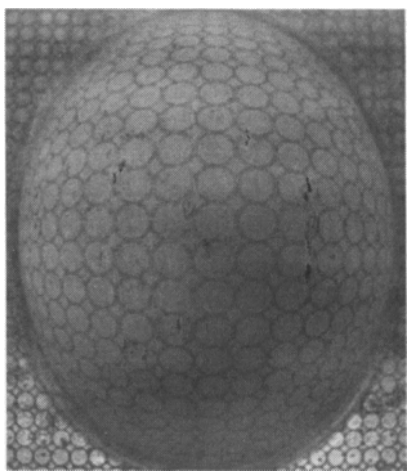

Figure 7. An example showing fracture at multiple locations in a domes formed out of sheet (N) at k = 0.8 in the 90° orientation.

The fracture surface of domes formed out of the four sheets (at k = 1.0) were closely examined by scanning-electron microscopy (SEM); samples of the obtained images are shown in Figure 8. Sheet (A) shows a regular ductile fracture, whereas sheet (N) exhibits material fracturing in multiple layers parallel to the sheet plane. Sheet (O) exhibits some tendency to fracture in layers like sheet (N), whereas sheet (M) is closer in fracture to sheet (A). The aforementioned layering of fractured surface is rather unusual. Therefore, analysis of a fragment between the fracture layers was performed using energy dispersive X-ray spectroscopy (EDS); the analysis revealed metal oxide particles. Furthermore, the optical micrographs in Figure 9 show second phase particle distribution in each of the four sheets, in the as-received condition. Sheets (A) and (M) display a uniform distribution of fine particles, which are mostly submicron in size. In addition to fine particles, sheet (N) exhibits agglomeration of the particles in the form of long (100-200 μm) stringers, parallel to the sheet rolling direction. A similar observation for Mg AZ31 sheet with a 2.0 mm initial thickness was made in the work of Carter et al. 2008 [23], although the morphology and chemistry of the stringers were not investigated in any detail. Sheet (O) shows some tendency for the second phase particles to align along the rolling direction, but nothing close to the level seen in sheet (N).

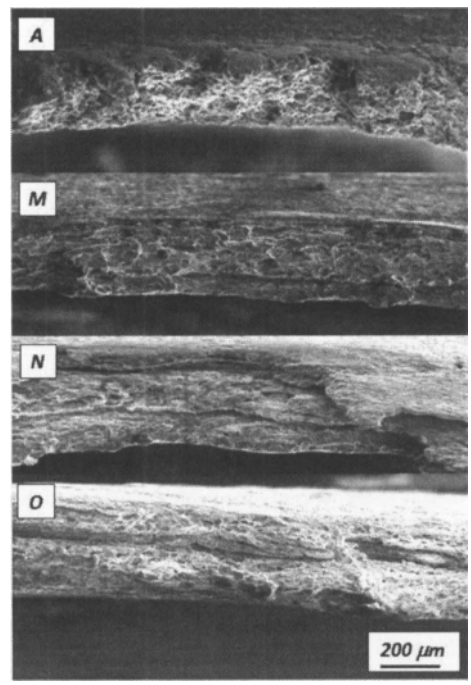

Figure 8. SEM images of fracture surfaces taken from domes formed out of the four Mg AZ31B sheets at (k = 1.0).

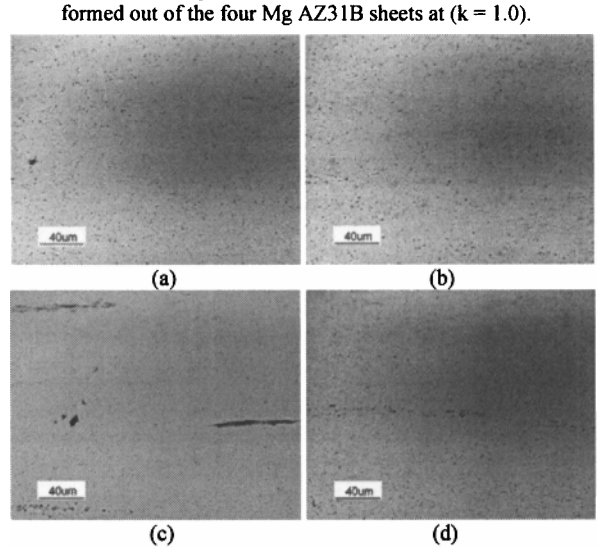

Figure 9. Optical micrographs (un-etched) of the four Mg AZ31B sheets showing second phase particles: (a) A (b) M (c) N (d) O.

EDS analysis of a stringer and a large particle in sheet (N) revealed the second phase to be essentially Mg oxide. It appears that sheet (N) has a significant amount of magnesium oxide that is not uniformly distributed in the microstructure. During elevated temperature forming, the close proximity of these oxide particles, present in the form of long stringers, makes it easier for the cavities formed at the oxide/matrix interface to coalesce and result in premature sheet failure. Failure occurring at multiple locations in sheet (N) corresponds to multiple stringers in the material; unlike the case with the (A, M and O) sheets, in which failure occurs at the dome pole strictly due to geometrical reasons.

Summary

A detailed investigation on the formability behaviors of four Mg AZ31 sheets (labeled A, M, N and O) was carried out under hot forming conditions (400 °C and $5x10^{-3}$ s^{-1}) using the pneumatic stretching test. For each sheet, friction-independent FLCs were constructed in two orientations; along and across the material's rolling direction. The 0° orientation showed greater formability limits than the 90° orientation for all four sheets. Comparison between the results obtained for the four sheets revealed that sheets (A) and (O), both produced by TRC casting and have a fine grain structure, outperformed the other two sheets. Sheet (M), the only one produced by DC casting, fell behind sheets (A) and (O), mainly due to its larger initial grain size. The formability limits of sheet (N) were found to be inferior to those of the other three sheets, despite its small initial grain size (~5 μm; similar to sheets (A) and (O)). In addition, excessive surface damage and fracture at multiple locations were observed in all the domes formed out of that particular sheet. This was shown to be the result of internal material defects in the form of long oxide stringers, which lead to premature failure and hence reduced formability limits.

References

1. J.A. Yasi, L.G. Hector, and D.R. Trinkle, "First-Principles Data for Solid-Solution Strengthening of Magnesium: From Geometry and Chemistry to Properties," *Acta Materialia*, 58 (2010) 5704-5713.

2. H. Li, E. Hsu, J. Szpunar, R. Verma, and J.T. Carter, "Determination of Active Slip/Twinning Modes in Mg Alloy Near Room Temperature," *Journal of Materials Engineering and Performance*, 16 (2006) 321-326.

3. J.T. Carter, V. Savic, L.G. Hector, A.R. Melo, and P.E. Krajewski, "Structural Evaluation of an Experimental Aluminum/Magnesium Decklid," SAE Paper No. 2011-01-0075.

4. E. Doege, and K. Dröder, "Sheet Metal Forming of Magnesium Wrought Alloys - Formability and Process Technology," *Journal Materials Processing Technology*, 115 (2001) 14-19.

5. S. Agnew, and O. Duygulu, "A Mechanistic Understanding of the Formability of Magnesium: Examining the Role of Temperature on the Deformation Mechanisms," *Materials Science Forum*, 419-422 (2003) 177-188.

6. F. Abu-Farha, and M. Khraisheh, "Analysis of Superplastic Deformation of AZ31 Magnesium Alloy," *Journal of Advanced Engineering Materials*, 9 (2007) 777-783.

7. F.K. Chen, and C.K. Chang, "Warm Stamping of Cell-Phone Cases with AZ31 Magnesium-Alloy Sheets," *Advanced Materials Research*, 154-155 (2010) 1826-1829.

8. S.P. Keeler, and W.A. Backofen, "Plastic Instability and Fracture in Sheets Stretched Over Rigid Punches," *ASM Transactions*, 56 (1963) 25-48.

9. ASTM E2218 – 2002, "Standard Test Method for Determining Forming Limit Curves".

10. Z. Marciniak, and K. Kuczynski, "Limit Strains in The Processes of Stretch-Forming Sheet Metal," *International Journal of Mechanical Sciences*, 9 (1967) 609-620.

11. K. Nakazima, T. Kikuma, and K. Asuka, "Study on the Formability of Steel Sheet," (Yawata technical report no. 264, 1971, 678-680).

12. "Metallic Materials - Guidelines for the Determination of Forming Limit Diagrams," (ISO 12004 1997).

13. E. Hsu, J. Carsley, and R. Verma, "Development of Forming Limit Diagrams of Aluminum and Magnesium Sheet Alloys at Elevated Temperatures," *Journal of Materials Engineering and Performance*, 17 (2008) 288-296.

14. T. Naka, G. Torikai, R. Hino, and F. Yoshida, "The Effects of Temperature and Forming Speed on the Forming Limit Diagram for Type 5083 Aluminum-Magnesium Alloy Sheet," *Journal of Materials Processing Technology*, 113 (2001) 648-653.

15. D. Li, and A. Ghosh, "Biaxial Warm Forming Behaviour of Aluminum Sheet Alloys," *Journal of Materials Processing Technology*, 145 (2001) 281-293.

16. F. Abu-Farha, L.G. Hector, and P.E. Krajewski, "Forming Limit Curves for the AA5083 Alloy under Quick Plastic Forming Conditions," SAE Paper No. 2011-01-0235.

17. F. Abu-Farha, and L.G. Hector, "Sheet Orientation Effects on the Hot Formability Limits of Lightweight Alloys," *ASME Journal of Manufacturing Science and Engineering*, In Press.

18. C. Dreyer, F. Polesak, T. Shultz, and S. Agnew, "Blind Study of the Effect of Processing History on the Constitutive Behaviour of Alloy AZ31B," *Proceedings of the 138th TMS Annual Meeting and Exhibition*, San Fransisco, CA (2009) 491-496.

19. R. Verma, J.T. Carter, and P.E. Krajewski, "High Temperature Deformation Behavior of Three Rolled Sheets of Magnesium Alloy AZ31," *Proceedings of the 138th TMS Annual Meeting and Exhibition*, San Francisco, CA (2009) 399-404.

20. D. Banabic, T. Balan, and D. Comsa, "Closed Form Solution for Bulging Through Elliptical Dies," *Journal of Materials Processing Technology*, 115 (2001) 83-86.

21. C.M. Sellars, and W.J. Tegart, "Relationship between Strength and Structure in Deformation at Elevated Temperature," *Mem. Sci. Rev. Metall.*, 63 (1967) 731-745.

22. L.T. Park, S.H. Myunga, D.H. Shin, and C.S. Lee, "Size and Distribution of Particles and Voids Pre-Existing in Equal Channel Angular Pressed 5083 Al Alloy: Their Effect on Cavitation during Low-Temperature Superplastic Deformation," *Materials Sci. & Eng. A*, 371 (2004) 178-186.

23. J.T. Carter, P.E. Krajewski, and R. Verma, "Hot Blow Forming of AZ31 Mg Sheet: Formability Assessment and Application Development," *JOM*, 60 (2008) 77-81.